Chapter 10

SWIFT AND ROAD UNEVENNESSES

10.1. Dynamic Tyre Response to Short Road Unevennesses

The actual road surface profile over which the tyre rolls may contain spectral components showing relatively short wavelengths. If the wavelength is smaller than two to three times the contact length a geometric filtering of the profile becomes necessary if the tyre model employed is assumed to contact the road in a single point. For the *SWIFT* model a special filter has been developed that takes care of the envelopment properties of the tyre and the variation in effective rolling radius that occurs when the tyre rolls over a short obstacle. The envelopment of an obstacle takes place in the contact zone. It is assumed that local dynamic effects can be neglected. The changing conditions that arise for the tyre, while quasi-statically traversing an obstacle, are measured and modelled and subsequently used as effective inputs for the tyre model also at higher speeds. The belt inertia takes care of the dynamic effects. The central item that is introduced is the effective road plane. Height, slopes and curvature of the effective surface are used as inputs in the tyre model. The orientation of the effective plane is defined such that the resulting force that would act on the assumedly frictionless road surface is directed normal to the effective road plane.

10.1.1. Tyre Envelopment Properties

In the literature one finds numerous publications on tyre envelopment behaviour. We refer to the study of Zegelaar (1998) for an extensive list of references. A number of these will be mentioned here. Important experimental observations have been made by Gough (1963). He indicated that the tyre that is slowly rolled at constant velocity and axle height, over a cleat with length much smaller than the contact length, exhibits three distinct responses: (1) variations in the vertical force, (2) variations in the (horizontal) longitudinal force and (3) variations in the angular velocity of the wheel. Lippmann et al. (1965,1967) studied the responses of both truck and passenger car tyres rolling over short sharp unevennesses like cleats and steps of several heights. From the experimental

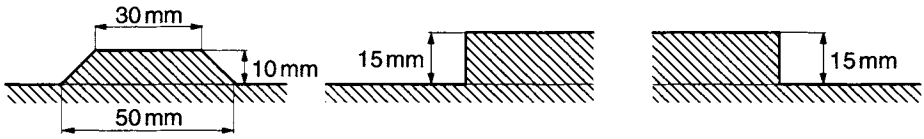

Fig. 10.1. Three typical obstacles used in Zegelaar's research.

observations it has been concluded that an almost linear relationship exists between tyre force variation and step height. The superposition principle may therefore be employed to assess the response to an arbitrarily shaped unevenness by taking the sum of responses to a series of step changes in road surface height. These observations are expected to be approximately true if the obstacle height is not too large.

For three typical road unevennesses, depicted in Fig.10.1, Zegelaar has measured the responses of the tyre at three different constant axle heights. To avoid dynamic effects, the velocity of the drum on which the cleat is attached (Fig.9.37) was maintained at the very low level of 0.2 km/h.

Figure 10.2 presents the measured vertical load F_V, horizontal longitudinal force F_H and the effective rolling radius r_e as derived from the measurements. The latter quantity is obtained from the variation of the wheel rotation rate $\mathrm{d}\theta/\mathrm{d}s$ which is defined as: the difference of the incremental wheel angular displacement and the constant (undisturbed) incremental rotation, as a ratio to the increment of the travelled distance of the wheel axle. The following equations apply:

$$r_e = \frac{V_x}{\Omega}, \quad V_x = \frac{\mathrm{d}s}{\mathrm{d}t}, \quad \Omega = \Omega_o - \frac{\mathrm{d}\theta}{\mathrm{d}t}, \quad r_{eo} = \frac{V_x}{\Omega_o} \tag{10.1}$$

and hence

$$r_e \approx r_{eo}\left(1 + r_{eo}\frac{\mathrm{d}\theta}{\mathrm{d}s}\right) \tag{10.2}$$

The peculiar shapes of the various response curves correspond very well with results found in the literature. Several tyre models have been used to simulate the experimental observations. Davis (1974) has developed a model featuring independent radial springs distributed along the circumference. By giving the individual springs a non-linear degressive characteristic the model is able to generate a vertical force response curve with the typical dip that shows up when running at relatively high initial loads. Badalamenti and Doyle (1988) developed a model also consisting of radial springs but now with additional interradial spring elements that connect the end points of adjacent radial springs in radial direction. When the deflections of neighbouring radial springs are not equal to

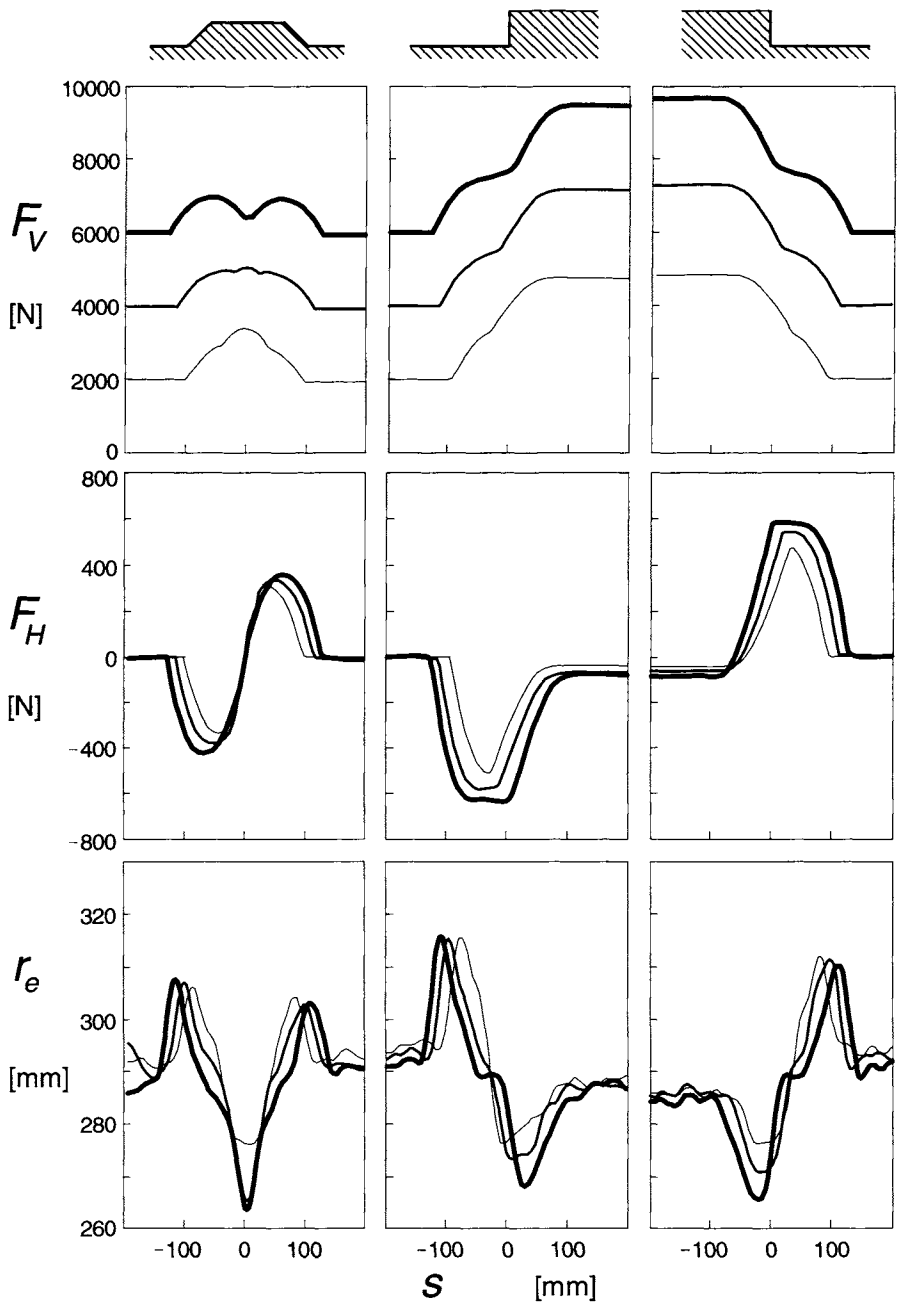

Fig. 10.2. Rolling over a trapezium cleat, an upward and a downward step (Fig.10.1) at very low speed and for three axle heights. Diagrams show measured variations of the vertical force F_V (upward +), the longitudinal horizontal force F_H (forward +) and the effective rolling radius r_e, Eq.(10.2). Tyre dimensions: 205/60R15.

each other, the interradial spring generates a radial 'shear force' that acts on the end points of the radial springs. Mousseau et al. (1994) and Oertel (1997) simulate the tyre rolling over a positive step by means of (different types of) finite element models; also cf. Gipser (1987,1999). Zegelaar uses the flexible ring (belt) model of Gong (1993), that was developed with the aid of the modal expansion method, as a reference model in his research. The addition of tread elements with radial and tangential compliances to Gong's model did enable Zegelaar to employ the model for the study of traversing obstacles. Also this model shows responses very similar to the measured behaviour. Schmeitz and Pauwellussen (2001) employ the radial interradial model as a possible basis for the pragmatic model running over an arbitrary road surface.

10.1.2. The Effective Road Plane

To arrive at a geometrically filtered road profile, Bandel follows the idea of Davis and introduces the effective road plane. The effective plane height and slope variation may be established by conducting an experiment where the wheel is rolled at a very low velocity over an uneven road surface at constant axle height (with respect to a horizontal reference plane) and the forces are measured, cf. Fig.10.3. It is argued that the resulting force (with the rolling resistance force omitted) that acts upon the wheel axle, is directed perpendicularly to the effective road plane. By dividing the variation of the measured vertical force, which is approximately equal to the vertical component of the normal force F_N, by the radial stiffness of the tyre, the effective height variation, $-w$, is obtained. The

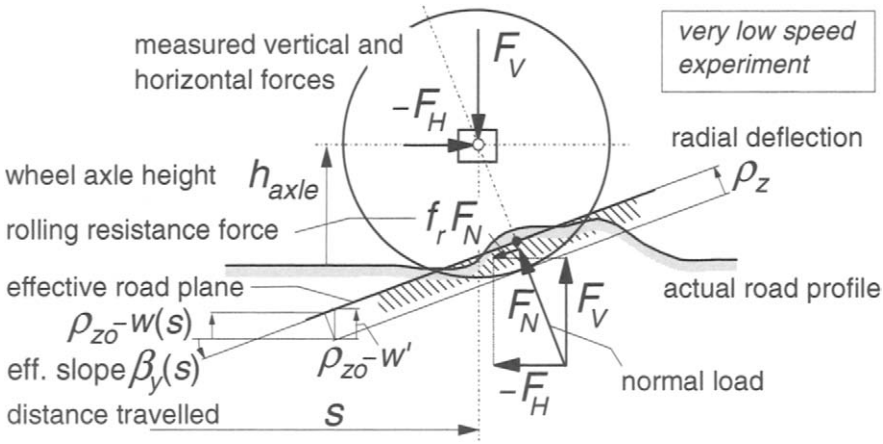

Fig. 10.3. The wheel rolled over a road irregularity at constant axle height to establish the effective road plane variation.

effective slope, $\tan\beta_y$, is found by dividing the longitudinal horizontal force (after having subtracted the relatively small rolling resistance force) by the vertical force. Both effective quantities are functions of the longitudinal position of the wheel centre s. The following formulae apply for the effective height w:

$$-w = \frac{F_V - F_{Vo}}{C_{Fz}} \approx \frac{F_N \cos\beta_y - F_{Vo}}{C_{Fz}} = \rho_z \cos\beta_y - \rho_{zo} \tag{10.3}$$

or for the actual effective height, w', defined as a vertical displacement, cf. Fig.10.3:

$$-w' = -w + \rho_z \tan\beta_y \sin\beta_y \tag{10.4}$$

For the effective forward slope $\tan\beta_y$ we have:

$$\tan\beta_y = -\frac{F_H + f_r F_N/\cos\beta_y}{F_V} \approx -\frac{F_H + f_r F_V}{F_V} \tag{10.5}$$

From Eq.(10.3) the approximate value (effect of small f_r disregarded) of the radial deflection ρ_z can be obtained. If needed, the actual effective road plane height, z_w, defined below the wheel spin axis, may be assessed, cf. Sec.10.1.6. For the description of the effective road input the pragmatic modelling approach initiated by Bandel et al. (1988) and further developed by Zegelaar and extended by Schmeitz is most useful and will be discussed below. Bandel discovered that the function representing the response of the change in vertical force to a short rectangular obstacle, featuring the dip at high load and the nipple at low load, can be decomposed into two identical basic functions, which are each others mirror image. The basic functions are found to be approximately independent of the initial tyre vertical deflection, that is: independent of the axle height. To find the force response curve at a possibly different axle height, the basic force curves are shifted with respect to each other over a distance a bit less than the contact length and then added together. By dividing by the radial stiffness of the tyre the basic height functions are found and from these the effective height variations w. For the ratio of the measured longitudinal force and vertical load variations a pair of basic functions can be assessed as well. Again, these are identical but the first must now be subtracted from the second to find the variation of the slope of the effective road plane $\tan\beta_y$, cf. Fig.10.4.

Zegelaar did experiments with the trapezium shaped cleat as indicated in Fig.10.1. He found basic functions which are practically symmetric in shape. Mirror imaging was not necessary and did certainly not apply for non-symmetric unevennesses such as the step. Also, the basic functions assessed for the vertical force appeared to be practically the same as the ones for the longitudinal force. These findings helped a lot to make the principle of the basic function easier and

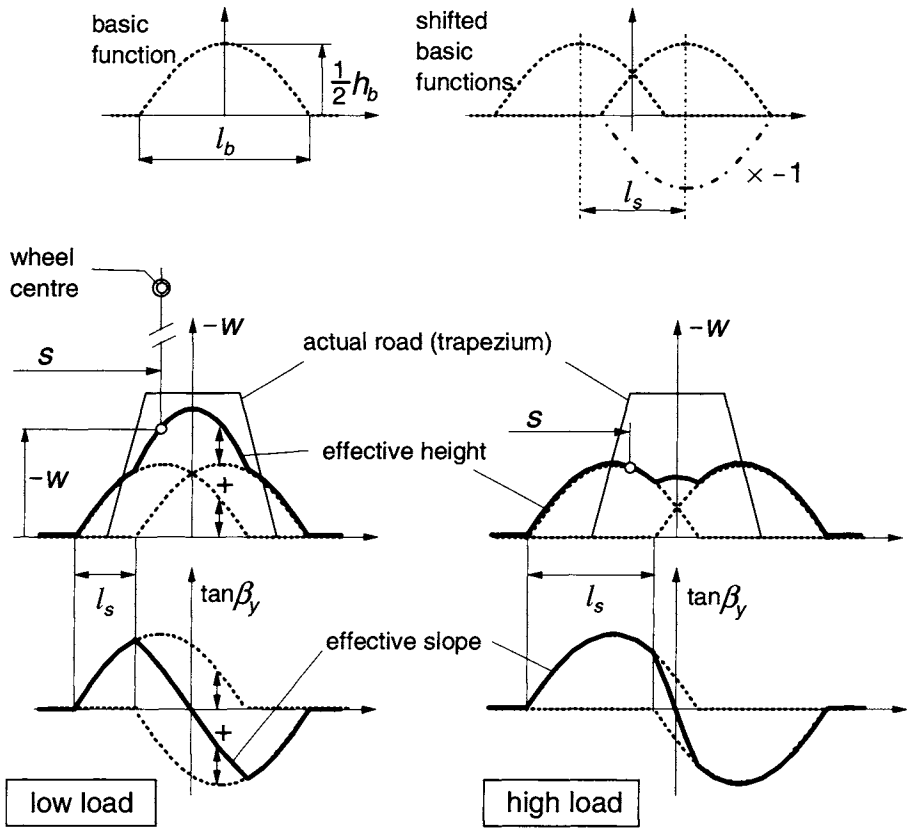

Fig. 10.4. The construction of the curves representing the effective height and effective slope from the basic function associated with the trapezium cleat.

more widely applicable. One basic function established from an experiment with a tyre rolling over a given road irregularity at a fixed constant axle position should be sufficient to serve as the source for assessing the equivalent road plane height and slope. These two equivalent quantities will later be extended with a third quantity: the effective forward road curvature that may significantly contribute to the variation of the effective rolling radius.

Figure 10.4 demonstrates the use of the basic function for the effective height applicable for the tyre rolling over a short trapezoidal cleat at a constant axle height. The vertical scale has been exaggerated. The basic function is approximated by a half sine wave. The base length of the curve is denoted with l_b, its height with $0.5h_b$ and the shift with l_s. The with travelled distance s varying values of w and β_y define the local effective road plane, cf. Sec.10.1.6. Figure 10.5 clarifies the actual situation. At wheel position s the current effective road

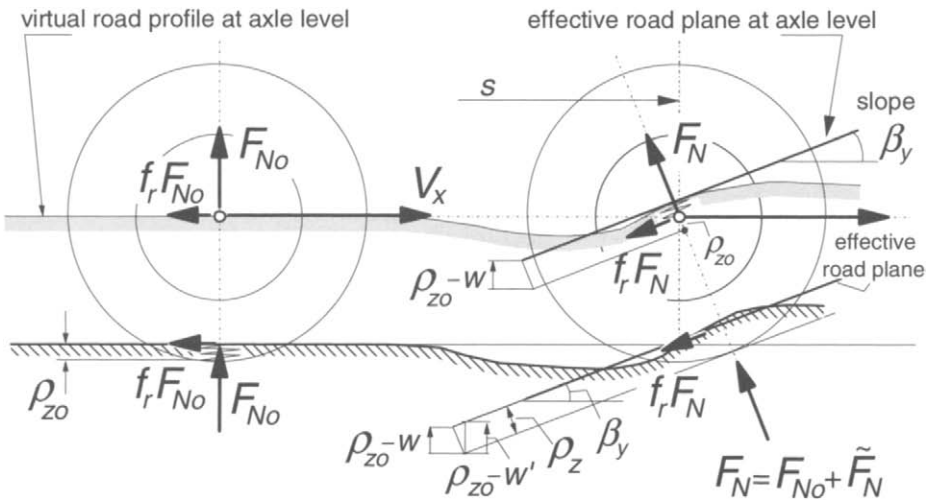

Fig. 10.5. The virtual road profile and effective road plane as sensed at wheel axle level.

plane has been indicated. The virtual road profile defined as the path of the wheel centre that would occur at constant normal load has been drawn together with the actual road profile. The distance of the wheel centre with respect to the virtual road profile corresponds to the increase of the actual radial tyre deflection. The distance of the wheel centre to the indicated effective road plane (translated to axle level with w and β_y regarded) is the increase in effective radial deflection which together with the initial deflection becomes equal to ρ_z.

10.1.3. The Two-Point Follower Technique

In Fig.10.6 an alternative technique is introduced using a single basic curve with full height h_b and a two-point follower. If the two points are moved along the basic curve the midpoint describes a curve that represents the characteristic for the effective height. The inclination angle of the follower corresponds to the slope of the effective road plane.

The response to a step change in road level may serve as a building block to compose the response to an arbitrary road unevenness. The corresponding basic function may be termed as the elementary basic function. The elementary basic curve may be represented by a quarter sine wave. For the steps given in Fig.10.1 the parameters of the basic curve have been determined by fitting the calculated force response to the vertical force variation measured for a series of axle heights (Fig.10.2).

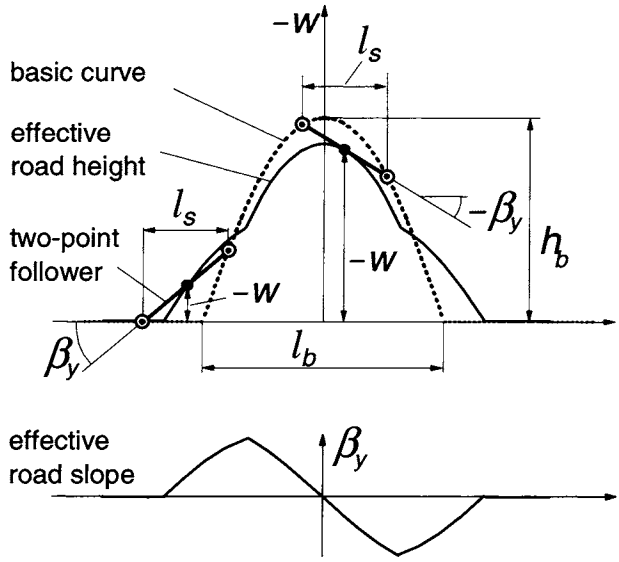

Fig. 10.6. Alternative method to determine the effective road height and slope using the basic curve with height h_b and the two-point follower with length equal to the shift l_s.

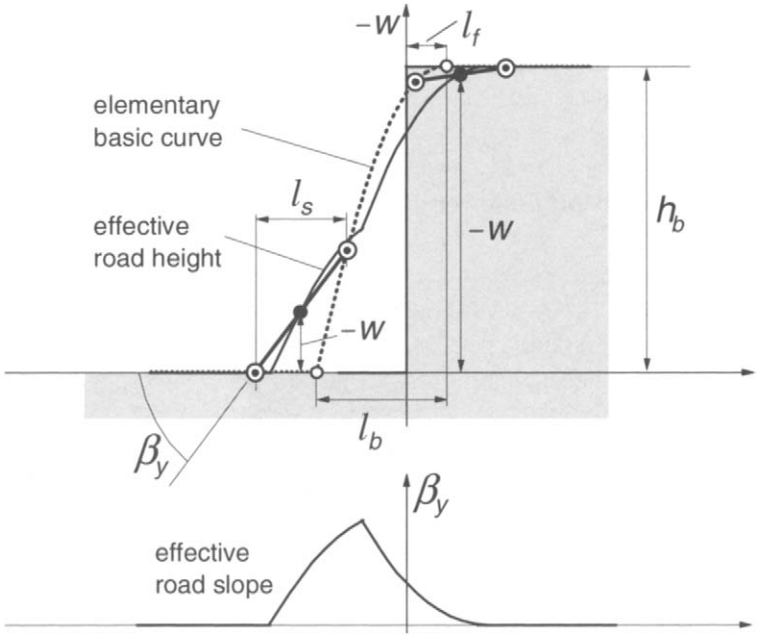

Fig. 10.7. The effective road response curves resulting from the (elementary) basic curve associated with the step change in road level by using the two-point follower concept.

Figure 10.6 shows the elementary basic curve for the upward step and the resulting effective road level and slope characteristics assessed by using the two-point follower technique. For the downward step the fitted basic function appears to come very close to the mirror image of the one determined for the upward step. The difference may very well be neglected. The parameters that control the size and position of the basic curve are the length l_b, the shift l_s and so-called offset l_f. The height h_b is equal to the step height. The offset is a new quantity that defines the position of the basic curve with respect to the step, cf. Fig.10.7.

A further important step is taken in the development of the assessment and use of basic functions. It is obvious that during the experiment that is performed at constant axle height, the normal load changes while rolling over an obstacle. The shift has been seen to change with axle height, that is: with a changed vertical load. The shift that corresponds to the length of the two-point follower has been found to be equal to a little less than the contact length. It seems therefore to be practical to adapt the strategy followed so far. We will henceforth define the basic curve to be assessed at constant vertical load. The experiments are to be carried out at constant load and at very low speed of travel. Schmeitz conducted such tests with the flat plank machine, cf. Sec.10.1.5. The effective height variation follows directly from the experiment. It turns out (cf. Sec.10.1.6) that w now simply equals the change in axle height, z_a. Division of the vertical force by the radial stiffness is not needed anymore which relieves us from accounting of a possibly non-linear tyre compression characteristic, cf. Eq.(9.220). In addition, since the rolling resistance is now assumed to remain constant, it is no longer necessary to take account of the rolling resistance force when determining the effective slope, as was done in Eq.(10.5).

Zegelaar calculated the step response with the flexible ring model provided with tread elements and found good agreement with measured data. By fitting the quarter sine curve representing the basic curve, parameter values have been assessed for a wide range of step heights. The results have been compared with the values calculated for a rigid wheel or zero normal load. Figure 10.8 illustrates the extreme case of the rigid wheel rolling over a step.

In Fig.10.9 Zegelaar's calculated results have been presented for a series of vertical loads F_V. The diagrams show that the basic curve length l_b and the offset l_f do change with step height h_{step} but are approximately independent of the vertical load F_V. The curve length may be estimated from the circle curve length, Fig.10.8:

$$l_b = \sqrt{r_o^2 - (r_o - h_{\text{step}})^2} \tag{10.6}$$

The horizontal shift l_s amounts to approximately 80% of the contact length $2a$.

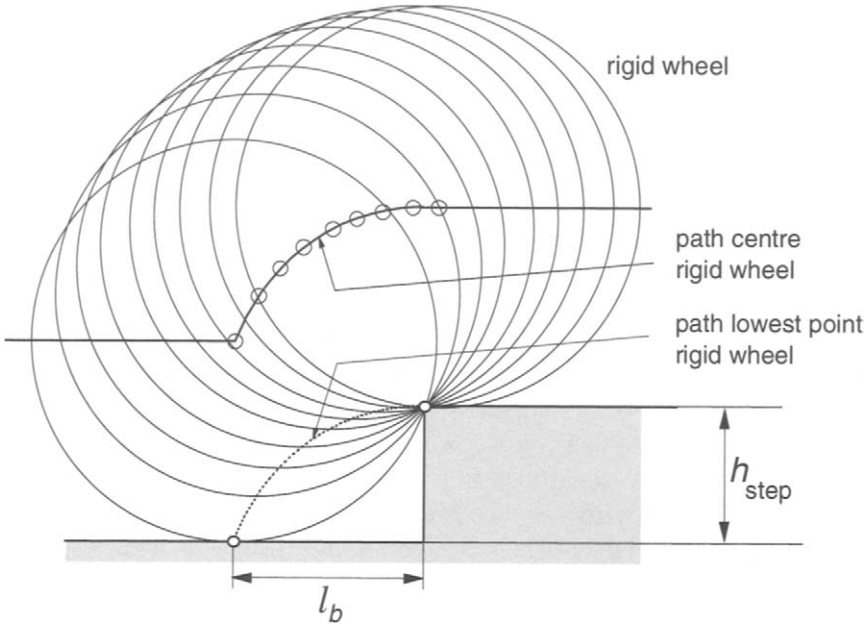

Fig. 10.8. The rigid wheel rolling over an upward step change in road level.

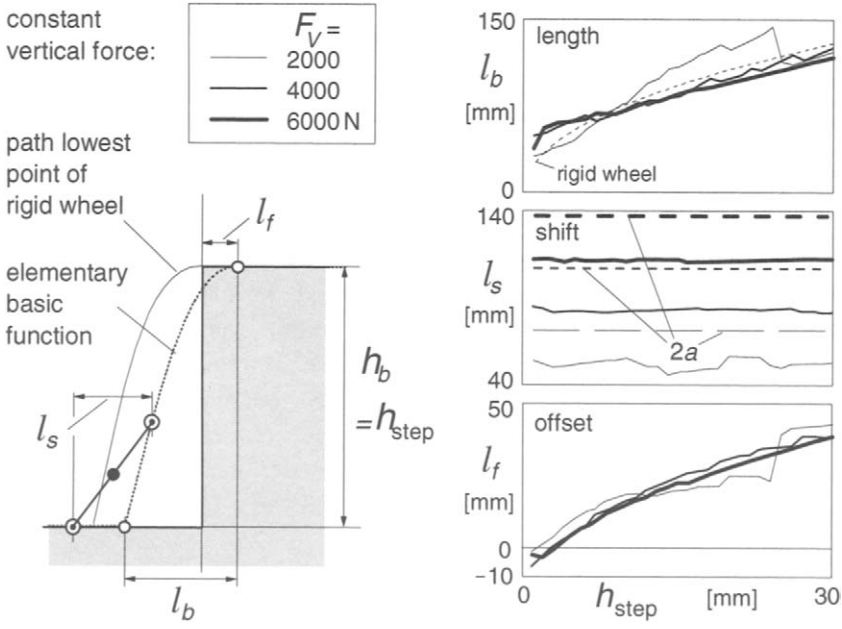

Fig. 10.9. Parameter values for the elementary basic curve established at constant vertical loads by computations using a flexible ring model with tread elements, Zegelaar (1998).

The offset may be approximated by a linear function becoming zero at vanishing step height.

The approach of employing basic curves to assess the effective road height and slope as inputs to the dynamic tyre model has been found adequate for the description of the response to single obstacles. Although, in principle, the method may be used also for a series of obstacles or for an arbitrary road surface profile with the elementary basic curve (that holds for a step unevenness) as building block, the rules that are to be followed may become rather cumbersome. For such a more general application the method developed by Schmeitz (2004), also cf. Schmeitz and Pacejka (2003), that is based on the so-called tandem cam technique is considered to be the best option.

The 'Tandem Cam' Technique

Instead of using the basic profile and running over that with the two-point follower we may more closely consider the actual tyre shape that moves over the road surface profile. Schmeitz discovered that the principle of the circle moving over the surface (Fig.10.8) may be adopted but than with an ellipse instead of the circle. This super ellipse that takes the shape of a standing egg has a height approximately equal to that of the tyre but a radius of curvature at the lowest point smaller than that of the free tyre. In that way, the 'cam' touches the step later than the circle would. By choosing an optimal shape of the ellipse, the role of the offset l_f (that changes with step height) of the sine based basic curve (Fig.10.9) can be taken care of automatically. Figure 10.10 depicts the cam moving over a step. The dimensions of the cam are defined by the super ellipse parameters. In terms of the coordinates x_e and z_e the ellipse equation reads:

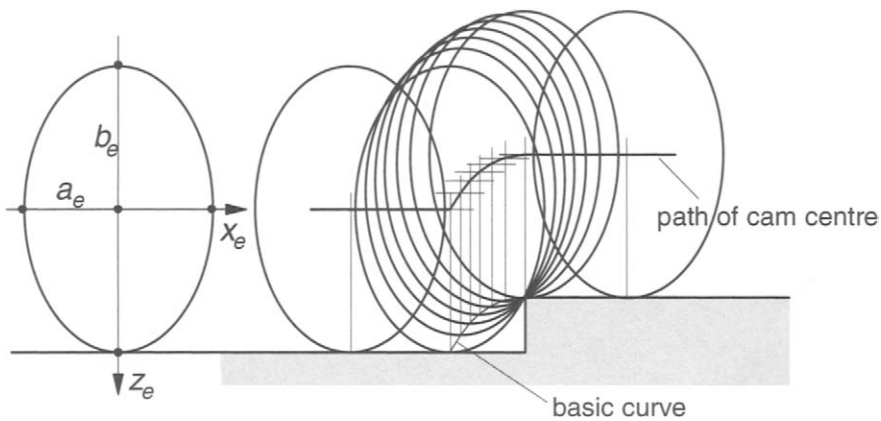

Fig.10.10. 'Cam' moving over step road profile, producing basic curve.

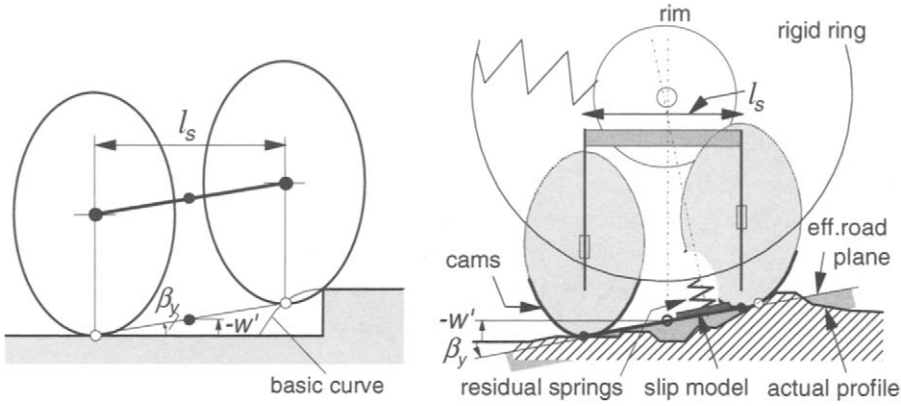

Fig. 10.11. The tandem cam configuration that generates the (actual) effective height and slope corresponding to the use of a basic curve and two-point follower. The total model including residual spring and rigid belt ring running over an arbitrary road profile.

$$\left(\frac{x_e}{a_e}\right)^{c_e} + \left(\frac{z_e}{b_e}\right)^{c_e} = 1 \tag{10.7}$$

The effective road height and slope can be assessed by using two cams following each other at a distance equal to the shift length l_s. The change in height of the midpoint of the connecting line and the inclination of this line represent the effective height and effective slope. Figure 10.11 illustrates this 'tandem cam' configuration. Fitting the tandem cam parameters follows from assessing the best approximation of low speed responses of a tyre running over steps of different heights at a number of constant vertical loads. Once the ellipse parameters have been established, the cam dimensions can be approximately considered to be independent of step height and vertical load. The tandem base

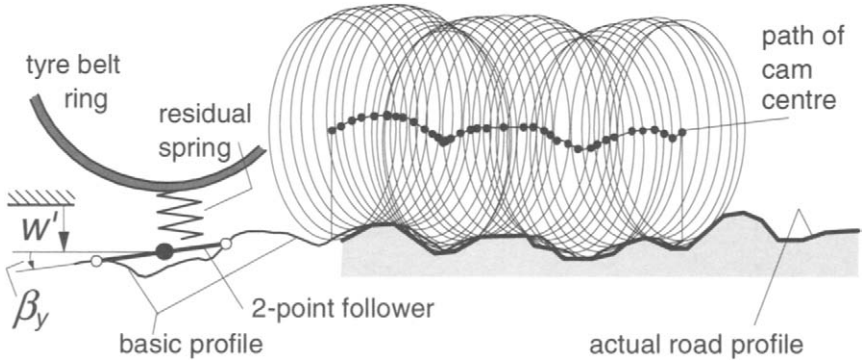

Fig. 10.12. The cam generating the basic road profile and two-point follower moving over it.

length l_s, however, does depend on the vertical load. It is interesting that analysis shows that the lower part of the ellipse turns out to be practically identical to the contour of the tyre in side view just in front of the contact zone up to the height of the highest step considered in the fitting process (Schmeitz 2004).

In a vehicle simulation, it may be more efficient to assess the basic profile first, that is: before the actual wheel rolls over the road section considered. This is achieved by sending one cam ahead over a given section of the road and having that determine the basic profile. The two-point follower is subsequently moved, concurrently with the actual wheel forward motion, over the basic profile, thereby generating the (actual) effective road inputs, w' and β_y which are fed into the tyre model. Figure 10.12 illustrates the procedure. When traversing a single step it is, of course, more efficient to use an analytic expression for the basic curve based on Eq.(10.7), cf. Fig.10.11 left.

10.1.4. The Effective Rolling Radius when Rolling over a Cleat

The third effective input is constituted by the effective road forward curvature that significantly changes the effective rolling radius when a road unevenness is traversed. In Fig.10.2 these variations have been shown in the lower diagrams. The curves are derived from measurements by using the Eqs.(10.1,10.2).

In the effort to model the aspect of rolling over an obstacle it is important to realise that we have three elements that contribute to the variation of the rolling radius:

1. increment in normal load
2. the local forward slope
3. the local forward curvature

Figure 10.13 illustrates the matter. The first item has been dealt with before, cf. Sec.8.3.1, Fig.8.12, Eq.(8.38) and Eq.(9.232). According to the latter equation the effective radius is a function of vertical load and speed of rolling. In Fig.10.14 model considerations and the graph resulting from experiments have

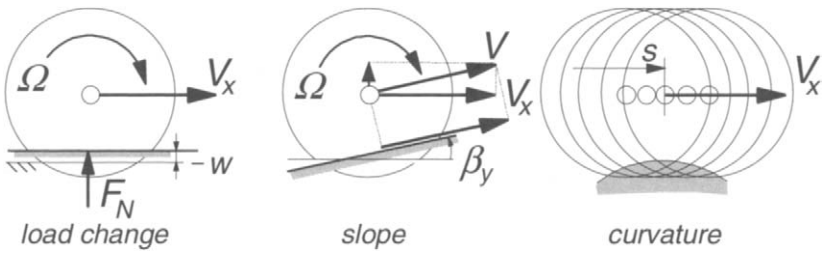

Fig. 10.13. Three contributions to the change in apparent effective rolling radius.

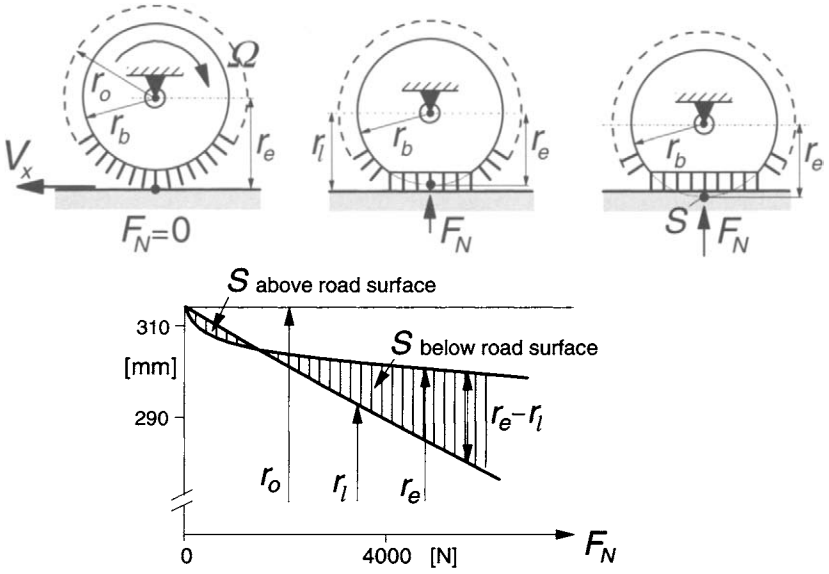

Fig. 10.14. The effective rolling radius varying with a change in normal load.

been repeated. For small variations in radial deflection we may employ the equation:

$$\tilde{r}_{e\eta} = -\eta\tilde{\rho}_z \tag{10.8}$$

The second contribution accounts for the fact that at a slope and unchanged normal load, the axle speed parallel to the road surface is larger than the horizontal component V_x. We have for the change in the apparent $r_e = V_x/\Omega$:

$$\tilde{r}_{e,\text{slope}} = -r_{eo}(1-\cos\beta_y) \tag{10.9}$$

The third contribution comes from the road surface curvature. The analysis that attempts to model the relation between curvature and effective rolling radius is more difficult and requires special attention. Figure 10.15 unravels the process of rolling over a curved obstacle and indicates the connection with rolling over a drum surface with same curvature. In contrast to the drum, the obstacle does not rotate. Consequently, to compare the process of rolling over a curved obstacle with that of rolling over a rotating drum surface, we must add the effect of the tyre supported by a counter rotating surface that does not move forwards. The left-hand diagram of Fig.10.16 depicts a possible test configuration with a plank that can be tilted about a transverse line in the contact surface. When being tilted, point *S*, that is attached to the wheel rim, must move along with the plank in longitudinal direction since the wheel slip is zero ($V_{sx}=0$) as brake or drive torque is not applied. Consequently, the wheel rotates slightly and the following

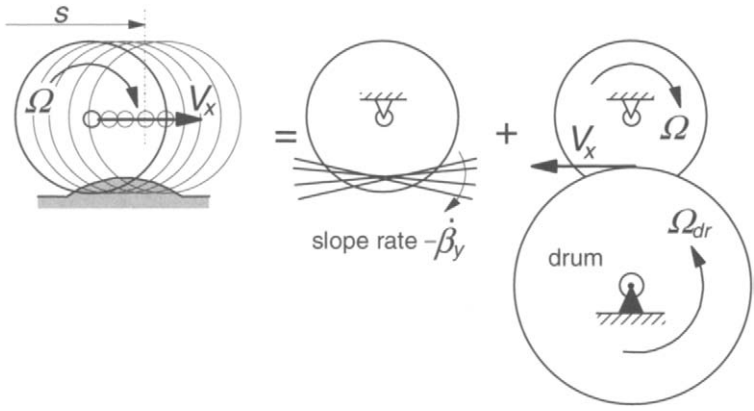

Fig. 10.15. Unravelling the process of rolling over a curved obstacle.

equation applies:

$$V_{sx} = -(r_{eo} - r_l)\frac{\mathrm{d}\beta_y}{\mathrm{d}t} - r_{eo}\tilde{\Omega} = 0 \tag{10.10}$$

The apparent variation in effective rolling radius derives from the equation:

$$\tilde{r}_e = \frac{V_x}{\Omega} - \frac{V_x}{\Omega_o} \approx -\frac{V_x}{\Omega_o^2}\tilde{\Omega} \tag{10.11}$$

so that we obtain for the contribution from the slope rate:

$$\tilde{r}_{e,\text{slope rate}} = \frac{r_{eo} - r_l}{\Omega_o}\frac{\mathrm{d}\beta_y}{\mathrm{d}t} \tag{10.12}$$

The relationship (10.10) has been confirmed to hold through elaborate experiments conducted by Zegelaar (1998) on the tilting plank of the Delft flat plank machine, cf. Fig.12.5.

The other contribution that comes from the drum analogue is found by considering the simple model shown in the right-hand diagram of Fig.10.16. The tread elements with length d_t are assumed to stand perpendicularly on the drum surface. The drum has a curvature with radius R_{dr}. The belt with radius r_b is considered inextensible. As a consequence we find the following relation between the wheel and drum velocities.

$$\Omega r_b = \Omega_{dr}(R_{dr} + d_t) = V_x\left(1 + \frac{d_t}{R_{dr}}\right) \tag{10.13}$$

and for the effective rolling radius for the tyre rolling freely over the drum surface:

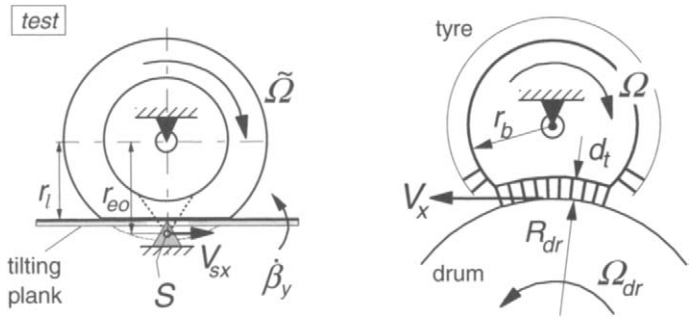

Fig. 10.16. Two components of rolling over a curved obstacle.

$$r_{e,\text{drum}} = \frac{V_x}{\Omega} = \frac{r_b}{1 + d_t/R_{dr}} \tag{10.14}$$

For the model, the effective rolling radius of the tyre rolling over a flat surface is equal to the radius of the belt:

$$r_{eo} = r_b \tag{10.15}$$

Now, the tread depth is:

$$d_t = r_o - r_{eo} \tag{10.16}$$

Hence, the expression for the effective rolling radius on the drum can be rewritten as:

$$r_{e,\text{drum}} = \frac{r_{eo}}{1 + (r_o - r_{eo})/R_{dr}} \approx r_{eo}\left(1 - \frac{r_o - r_{eo}}{R_{dr}}\right) \tag{10.17}$$

The variation of the radius becomes:

$$\tilde{r}_{e,\text{drum}} = -(r_o - r_{eo})\frac{r_{eo}}{R_{dr}} \tag{10.18}$$

The drum radius is equal to the radius of curvature of the (effective) road surface profile. This curvature corresponds to change in slope β_y with travelled distance s. Note that for the convex drum surface the β_y rate of change is negative. So, we have:

$$\frac{1}{R_{dr}} = -\frac{\mathrm{d}\beta_y}{\mathrm{d}s} \tag{10.19}$$

The slope rate of change may be written as:

$$\frac{\mathrm{d}\beta_y}{\mathrm{d}s} = \beta_y' = \frac{1}{V_x}\frac{\mathrm{d}\beta_y}{\mathrm{d}t} = \frac{1}{\Omega_o r_{eo}}\frac{\mathrm{d}\beta_y}{\mathrm{d}t} \tag{10.20}$$

The drum contribution is now expressed as:

$$\tilde{r}_{e,\text{drum}} = \frac{r_o - r_{eo}}{\Omega_o} \frac{\mathrm{d}\beta_y}{\mathrm{d}t} \tag{10.21}$$

Adding up the two contributions (10.12) and (10.21) yields the variation in effective rolling radius due to obstacle curvature:

$$\begin{aligned} \tilde{r}_{e,\text{curvature}} &= \tilde{r}_{e,\text{slope rate}} + \tilde{r}_{e,\text{drum}} \\ &= \frac{r_o - r_l}{\Omega_o} \frac{\mathrm{d}\beta_y}{\mathrm{d}t} = \rho_z r_{eo} \frac{\mathrm{d}\beta_y}{\mathrm{d}s} \end{aligned} \tag{10.22}$$

where ρ_z is the radial compression of the tyre. By adding up all the contributions we finally obtain for the variation of the effective rolling radius with respect to the initial condition where $\beta_y = \mathrm{d}\beta_y/\mathrm{d}s = 0$ and $\rho_z = \rho_{zo}$:

$$\tilde{r}_e = -\eta\tilde{\rho}_z - r_{eo}(1 - \cos\beta_y) + \rho_z r_{eo} \frac{\mathrm{d}\beta_y}{\mathrm{d}s} \tag{10.23}$$

The term with the effective forward curvature $\mathrm{d}\beta_y/\mathrm{d}s$ constitutes by far the most important contribution to the effective rolling radius variation and thus to the wheel rotational acceleration that can only be brought about by a variation in the longitudinal force F_x. This force also often outweighs the part of the horizontal longitudinal force F_H that directly results from the slope itself, cf. (10.5).

The effective curvature $\mathrm{d}\beta_y/\mathrm{d}s$ may show abrupt changes at the beginning and end of the passage over an obstacle. To assess the curvature and at the same time smoothen the discontinuities of the response we may send β_y through a first-order filter, Eq.(10.24), with 'time constant' σ_β/V_x. After taking the difference of input β_y and output y and dividing by the length σ_β, the filtered curvature $\mathrm{d}y/\mathrm{d}s$ is obtained, Eq.(10.25), that vanishes at wavelengths approaching zero.

$$\frac{\sigma_\beta}{V_x} \frac{\mathrm{d}y}{\mathrm{d}t} + y = \beta_y \tag{10.24}$$

$$\frac{\mathrm{d}y}{\mathrm{d}s} = \frac{\beta_y - y}{\sigma_\beta} \tag{10.25}$$

10.1.5. Simulations and Experimental Evidence

Zegelaar and Schmeitz have performed numerous experiments on the drum test stand (Fig.9.37) and the flat plank machine (Figs.10.17 and 12.5) and used the *SWIFT* model (including enveloping model) to carry out the simulations. Figure 10.9 shows the obstacle parameter values for the quarter sine basic curve of Zegelaar. Table 10.1 gives the parameters used by Schmeitz which are based on the ellipse concept (tandem cam technique).

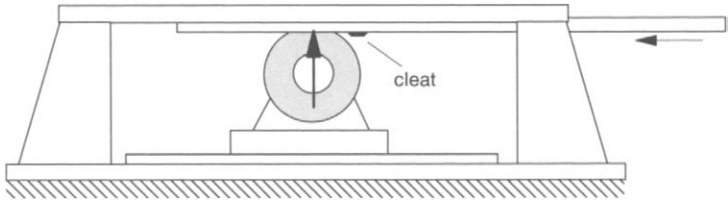

Fig. 10.17. Principle of the flat plank machine provided with a trapezium shaped cleat.

Table 10.1. Parameter values used for envelopment calculations. Tyre: 205/60R15, 2.2bar

unloaded radius	r_o	0.310 m
effective rolling radius at F_N= 4000N	r_{eo}	0.305 m
slope effective rolling radius characteristic	η	0.3
vertical tyre stiffness at F_N= 4000N	C_{Fz}	220 N/mm
rolling resistance, cf. Eqs.(9.230,9.231)	q_{sy1}	0.01
half contact length, cf. Eq.(9.207)	a	cf. Table 9.3
half ellipse length/unloaded radius a_e/r_o	p_{ae}	1.0325
half ellipse height/unloaded radius b_e/r_o	p_{be}	1.0306
ellipse exponent c_e	p_{ce}	1.8230
shift length /contact length $l_s/2a$	p_{sh}	0.8773

The table shows that the height and length of the ellipse are slightly larger than the dimensions of the free tyre. It is the exponent that gives rise to the larger curvature of the ellipse near the ground.

Figure 10.18 presents the measured and calculated variations of the actual effective height $-w'$, the horizontal fore and aft force F_H and the effective rolling radius r_e with the vertical load kept constant while slowly rolling over the trapezium cleat. The effective road plane slope $\tan\beta_y$ follows from the ratio of the horizontal force variation and the vertical load. The calculations are based on the two-cam tandem concept of Fig.10.11. The tandem is moved over the original road profile and the effective height and slope are obtained. From the derivative of β_y the effective rolling radius is found by using Eq.(10.23) which also contains the two very small additional contributions. It is observed, that a good agreement between test and calculation results can be achieved. The use of the quarter sine basic curve function gives very similar results.

Figures 10.19-23 present the results of rolling over the same cleat at different

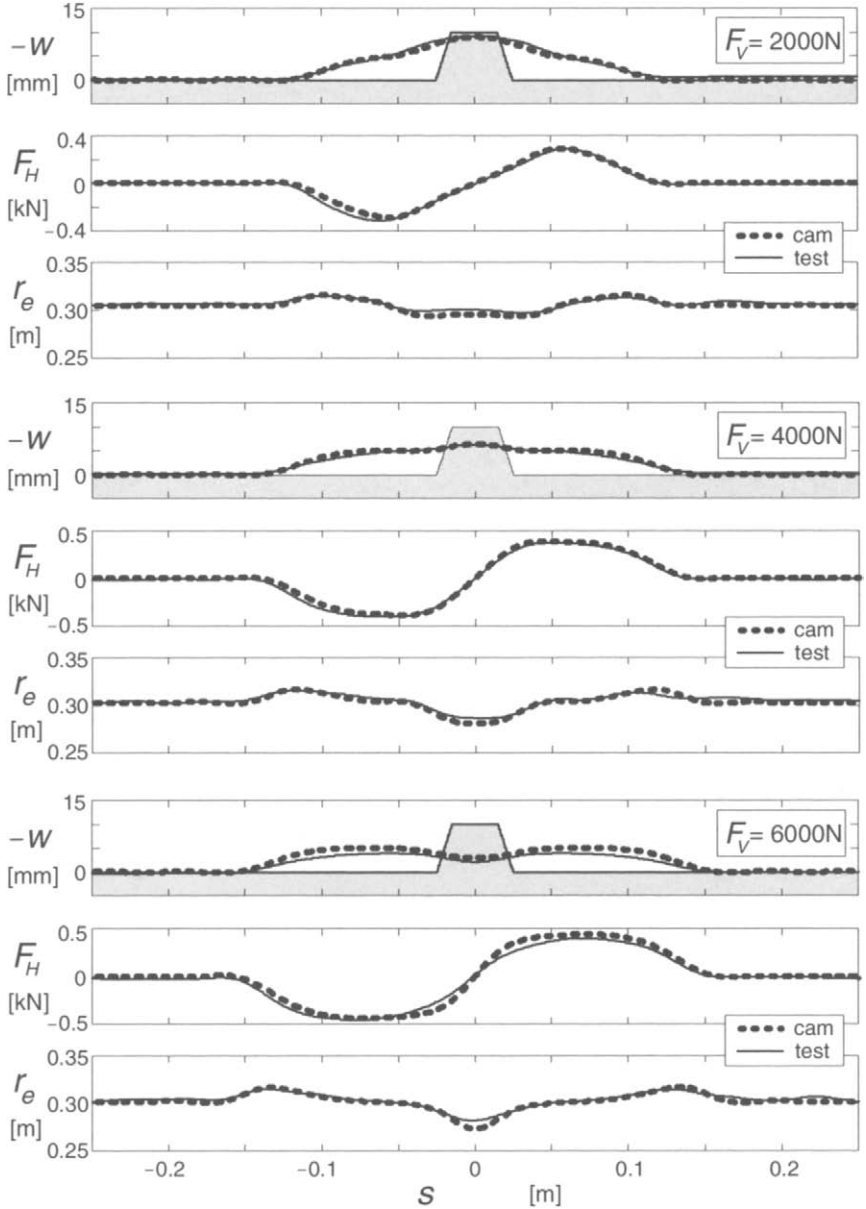

Fig. 10.18. Rolling over a trapezium cleat (length:50mm, height: 10mm). Measured and calculated variation of vertical axle displacement, horizontal longitudinal force and effective rolling radius at three different constant vertical loads. Measurements carried out on the Delft flat plank machine (very low speed) and calculations conducted with the use of the tandem cam technique (Fig.10.11) and Eq.(10.22). Tandem cam parameters according to Table 10.1.

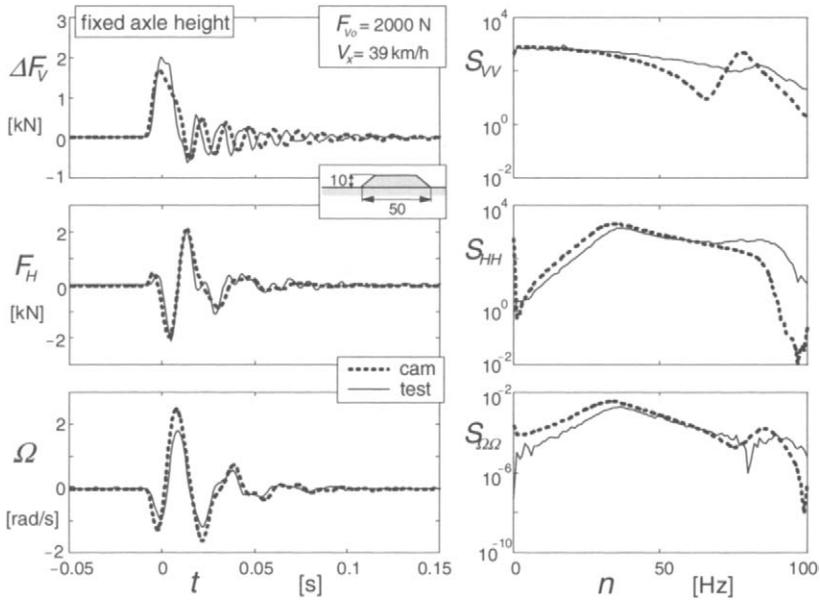

Fig. 10.19. Time traces and power spectra of vertical force, horizontal longitudinal force and angular velocity for wheel running at given speed of 39 km/h and initial vertical load of 2000 N over trapezium cleat at constant axle height using *SWIFT* tyre parameters and obstacle parameters of Table 10.1. (Schmeitz).

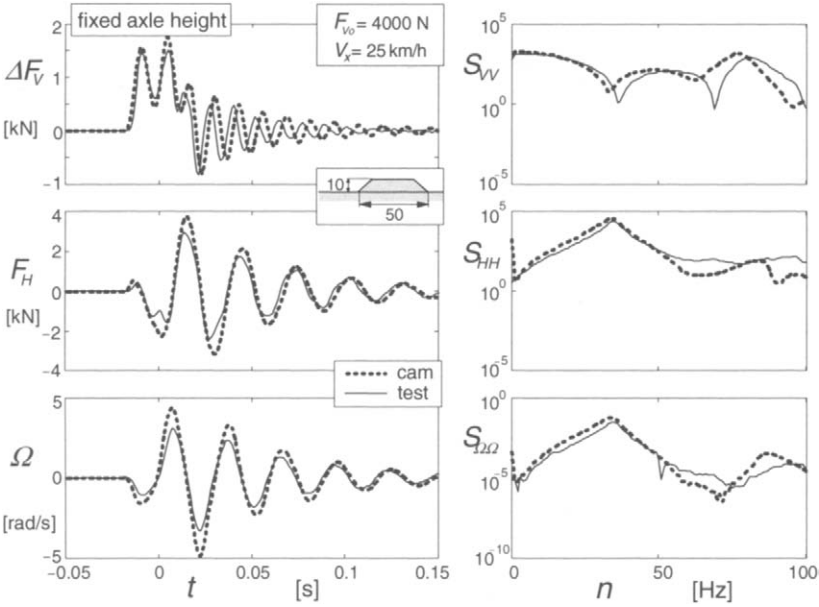

Fig. 10.20. Same as Fig.10.19 but at different speed and initial vertical load .

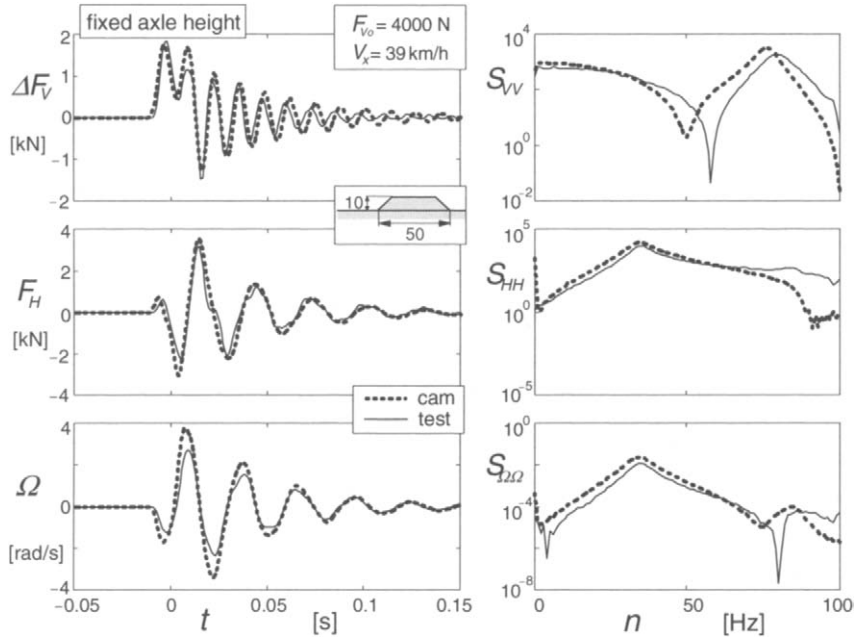

Fig. 10.21. Same as Fig.10.20 but at different speed.

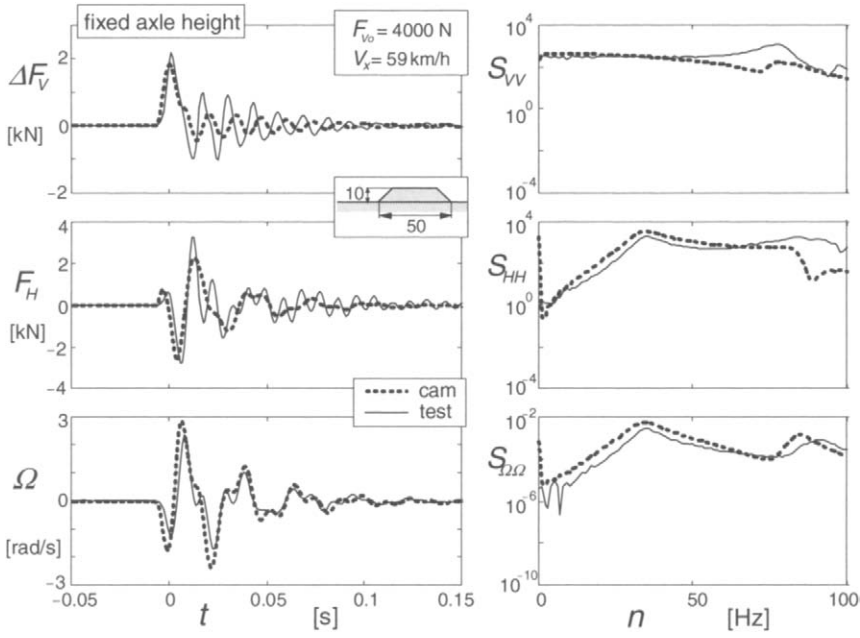

Fig. 10.22. Same as Fig.10.21 but at different speed.

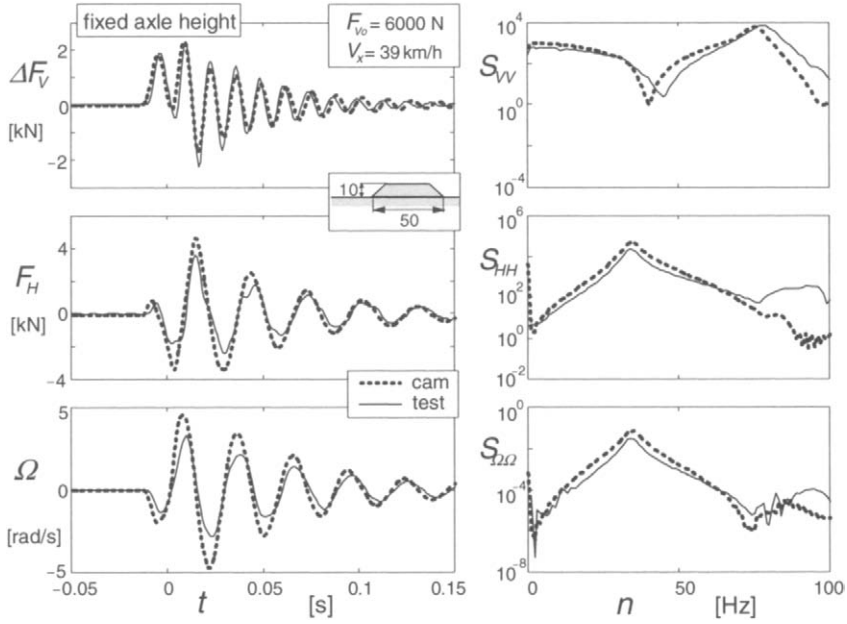

Fig. 10.23. Same as Fig.10.21 but at different initial vertical load .

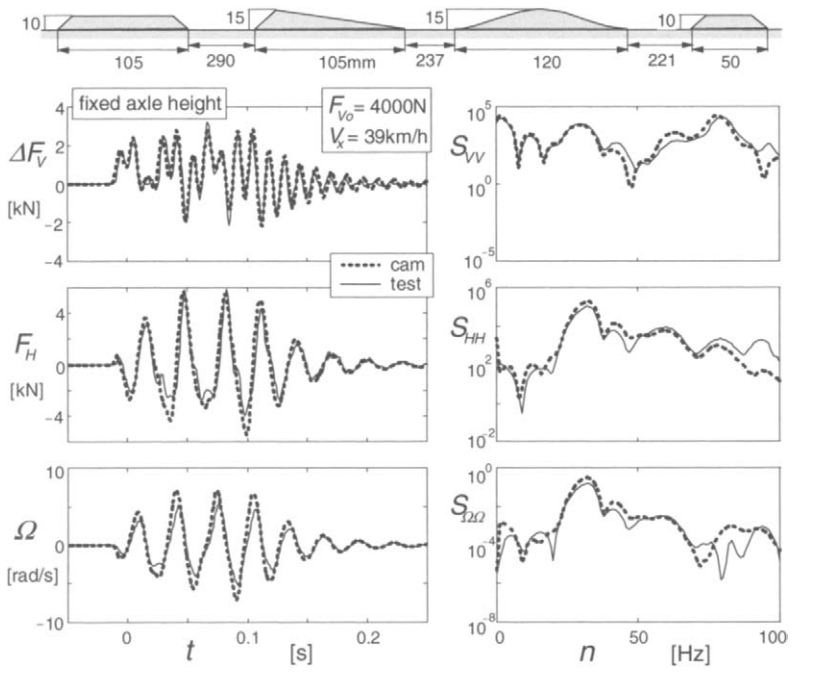

Fig. 10.24. Running over a series of cleats mounted on drum surface, at constant axle height.

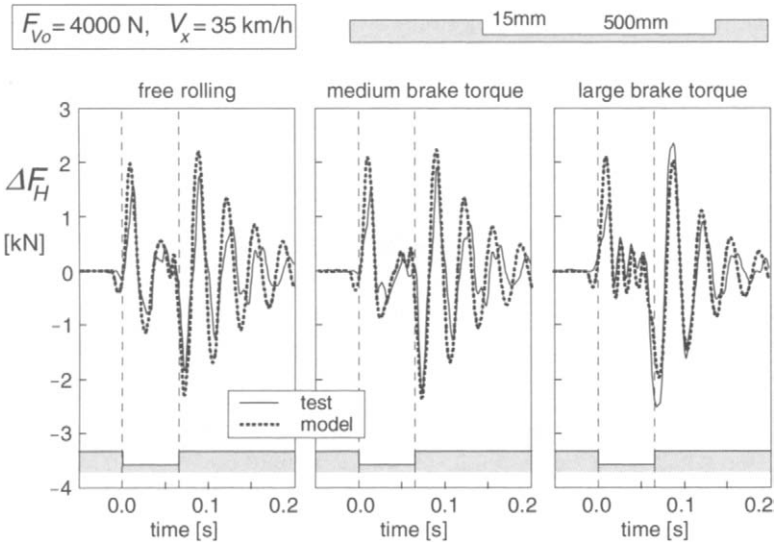

Fig. 10.25. The horizontal force variation when traversing a pothole while the wheel is being braked at three different levels of brake torque (M_B = ca. 4, 375, 850Nm respectively, Zegelaar 1998). Experiments on 2.5m drum, calculations using parameters according to Fig.10.9.

speeds while the axle location is kept fixed. The responses of the vertical, fore and aft forces and the wheel angular speed have been indicated. In addition, the power spectra of these quantities have been shown. Especially at the higher loads the calculated responses appear to follow the measured characteristics quite well up to frequencies around 50Hz or higher. Figure 10.24 demonstrates the application to a more general road surface profile. It shows the responses of the tyre when moving over a series of different types of cleats that resembles an uneven stretch of road.

Finally, in Fig.10.25 the test and simulation results conducted by Zegelaar (1998) have been depicted, representing a more complex condition where the tyre is subjected to a given brake torque (brake pressure) while the wheel rolls over a pothole at fixed axle location. The complex longitudinal force response conditions that are brought about by load and slip variations induced by tyre modal vibrations and road unevennesses are simulated quite satisfactorily using the *SWIFT* model including obstacle geometric filtering.

10.1.6. Effective Road Plane and Road and Wheel Camber

Before introducing the more complex situation of road camber in addition to forward slope and thereafter the inclusion of wheel camber, a more precise

account will be given of the notion of the effective road plane with a clear definition of the effective road plane height.

Effective Road Plane Height

In Figs.10.3 and 10.5 the effective height -w is considered as being assessed at a constant axle height above the reference plane that coincides with the initial flat level road surface. In Fig.10.26 the alternative case is illustrated where the effective height is assessed at constant vertical load F_V. The following formula covers both cases. The effective height is defined as:

$$w = z_a - \rho_{zV} \tag{10.26}$$

where z_a denotes the vertical axle displacement and ρ_{zV} the vertical tyre deflection when loaded on a flat level road with load F_V. With an assumed linear tyre spring characteristic we get:

$$\rho_{zV} = F_V / C_{Fz} \tag{10.27}$$

For the case that the effective height is found at a constant vertical load F_V, the initial vertical deflection is $z_{a0} = \rho_{zo} = \rho_{zV}$. Consequently, by considering (10.26), the variation in effective height equals the change in axle height.

If the axle height is kept constant, we have $z_a = z_{a0} = \rho_{zo}$ and the formula becomes: $w = \rho_{zo} - \rho_{zV}$ which corresponds with Eq.(10.3).

In Fig.10.26 the actual position of the effective road plane is defined as the location of the point of intersection of effective road plane and the vertical line through the centre of the vertical wheel. Its height below the horizontal reference plane is designated as z_w.

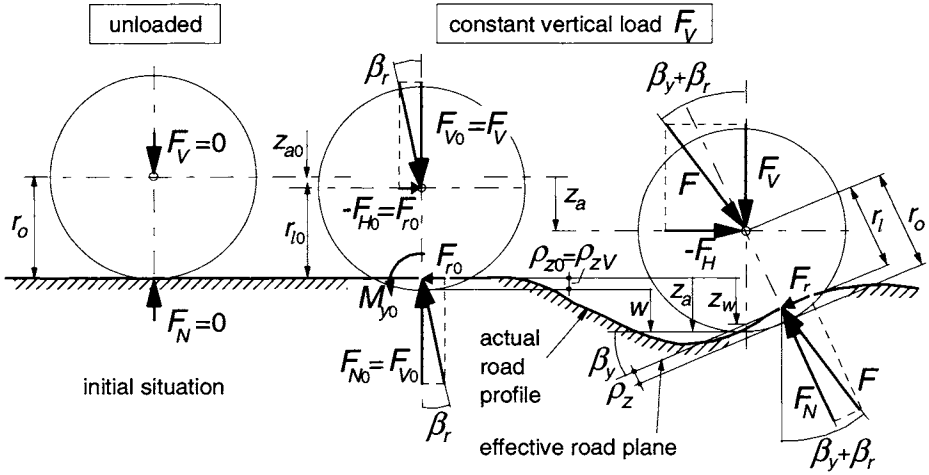

Fig. 10.26. The effective road plane assessed at constant vertical load.

With the small effect of the rolling resistance force $F_r = f_r F_N$ first included and then neglected, the normal force becomes in terms of the vertical load:

$$F_N = \frac{F_V}{\cos\beta_y - f_r \sin\beta_y} \approx \frac{F_V}{\cos\beta_y} \tag{10.28}$$

Consequently, the normal deflection becomes:

$$\rho_z = \frac{F_N}{C_{Fz}} = \frac{\rho_{zV}}{\cos\beta_y - f_r \sin\beta_y} \approx \frac{\rho_{zV}}{\cos\beta_y} \tag{10.29}$$

The effective road plane height follows from Fig.10.26 by inspection and reads:

$$z_w = w - \frac{\rho_z}{\cos\beta_y} + \rho_{zV} + r_o \frac{1-\cos\beta_y}{\cos\beta_y} \approx w - \rho_{zV}\tan^2\beta_y + r_o \frac{1-\cos\beta_y}{\cos\beta_y} \tag{10.30}$$

After introducing the actual effective height w' and using (10.26) and (10.29):

$$w' = w - \frac{\rho_z}{\cos\beta_y} + \rho_{zV} \approx w - \rho_{zV}\tan^2\beta_y = z_a - \frac{\rho_{zV}}{\cos^2\beta_y} \tag{10.31}$$

the expression for the effective road plane height becomes:

$$z_w = w' + r_o \frac{1-\cos\beta_y}{\cos\beta_y} \tag{10.32}$$

Obviously, on a flat sloping road surface the height z_w does not depend on the vertical load, that is on ρ_{zV}. As a consequence, it follows from (10.30) that the effective height w does depend on the vertical load. To avoid this load dependency, the actual effective height w' has been introduced. Equation (10.31) defines the relationship between the two quantities. Equation (10.32) shows that the effective road plane is located slightly lower than the height of the middle of the tandem cam connection line that is defined as $-w'$ indicated in Figs.10.1 and 10.12.

After having established the actual effective height and slope, e.g. by using the tandem cam technique, the normal tyre compression and loaded radius can be calculated by using Eqs.(10.29,10.31). We obtain for the loaded radius at given vertical axle location z_a and influence of the rolling resistance neglected:

$$r_l = r_o - (z_a - w')\cos\beta_y \tag{10.33}$$

We may use Eq.(9.218) or (7.46) to find the normal deflection ρ_z (for now at wheel camber $\gamma = 0$). It is seen, that the effective road plane height z_w is not needed to determine the deflection and that the actual height w' suffices.

Road and Wheel Camber

With the effective road plane height properly defined, we can now introduce a road transverse slope. By considering a tilt angle of the effective road plane

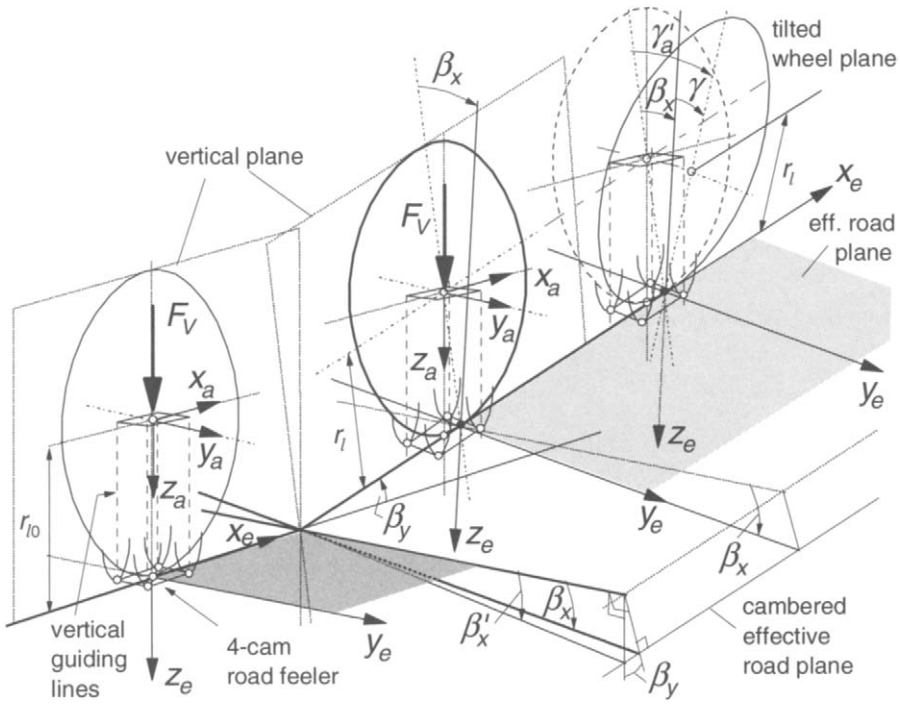

Fig. 10.27. The effective road plane showing forward and transverse slope angles β_y and β_x. Wheel plane in vertical and in tilted position. Road feeler senses angles β_y and β'_x.

brought about by rotating around the line of intersection with the wheel centre plane, that is about the x_e axis, the loaded tyre radius r_l remains unaffected. It may be noted, as indicated in the figure, that the thus obtained road camber angle β_x is slightly different from the transverse slope angle β'_x that may be defined as the angle between the horizontal wheel spin axis and the line of intersection of the effective road plane and the vertical plane through the wheel spin axis. We have the relation: $\tan\beta'_x = \tan\beta_x / \cos\beta_y$.

As indicated in the middle diagram, the transverse slope may be detected by a double track tandem cam 'road feeler'. The four cams are guided along vertical lines that are positioned symmetrically with respect to the two vertical planes, one passing through the wheel spin axis and the other through the line of intersection of the wheel centre plane and the horizontal plane that may be approximately defined to pass through the lowest point of the tyre undeformed peripheral circle, that is at a distance equal to r_o from the wheel centre.

In case we have a tilted wheel, again by rotating the wheel around the line of intersection, that is around the x_e axis, the road feeler is oriented at a slightly different yaw angle and the detected road transverse slope differs a bit from β'_x.

The case of combined road and wheel camber is illustrated in the right-hand

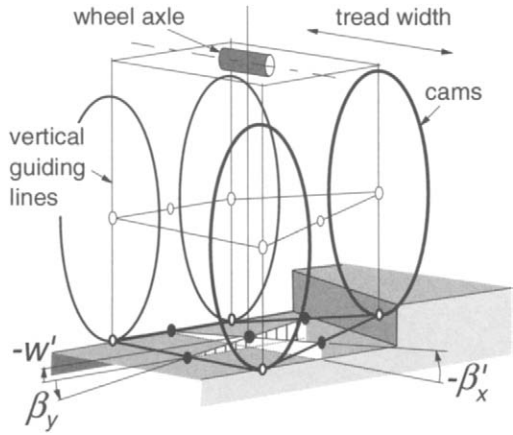

Fig. 10.28. The double-track tandem-cam road feeler moving over an oblique step.

diagram of Fig.10.27. The tyre camber angle γ (relative to the road plane) results from subtracting the wheel axle tilt angle γ'_a and the road plane camber angle β_x. It may again be noted that γ'_a differs from the global wheel inclination angle γ_a defined about a horizontal x axis. In the presence of wheel camber, the loaded radius results from the adapted Eq.(10.33):

$$r_l \cos\gamma'_a = r_l \cos(\gamma + \beta_x) = r_o - (z_a - w')\cos\beta_y \qquad (10.34)$$

Equation (9.218) or (7.46) can now be used to obtain the normal deflection ρ_z but now with tyre camber angle γ included.

In Fig.10.28 the situation is depicted for an upright wheel rolling over an oblique step. Schmeitz has conducted extensive experimental and model studies for a tyre rolling over such types of non-symmetric road unevennesses. For more information we refer to Schmeitz (2004), and Schmeitz and Pacejka (2003). To achieve more accurate results, additional cams (say three) may be inserted along

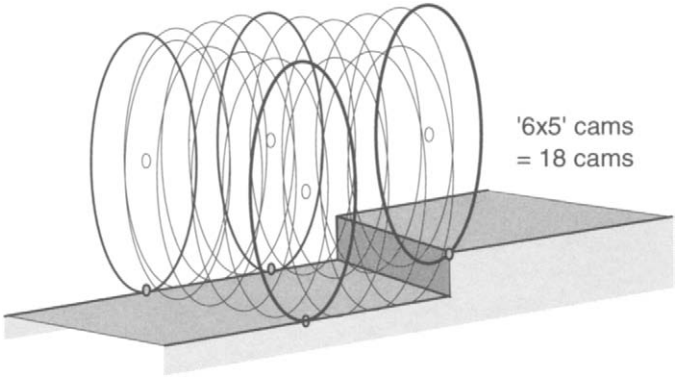

Fig. 10.29. Road feeler with more cams on the four edges to improve accuracy.

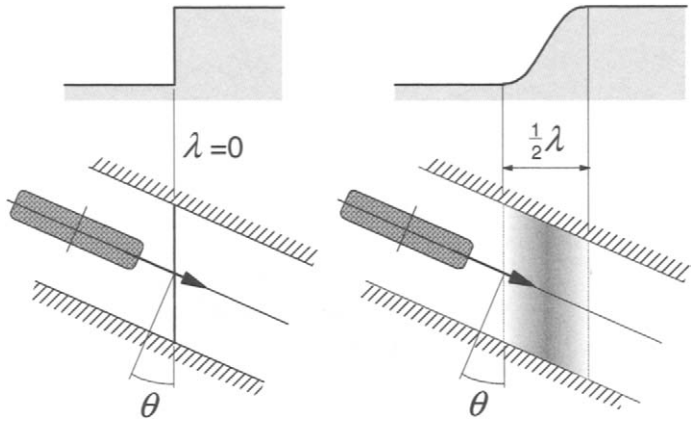

Fig. 10.30. Oblque step with zero and larger 'wavelength'.

the four edges (with calculated slopes averaged) when running over non-symmetrical obstacles, such as oblique steps or strips, Fig.10.29, exhibiting transverse slope variations with short wavelength (<ca.0.2m), see Fig.10.30.

The inclusion of the non-lagging part, as discussed in Sec.7.2.4, is needed to get good agreement with low speed flat plank test results. The effect shows up when the effective road plane changes in height and exhibits a varying transverse slope angle β_x, cf. Fig.10.31. The expressions for the two side slip velocity components parallel to the local effective road plane, cf. Eqs.(7.42a,b), now contain a term that originates from the effective road warp $d\beta_x/ds$:

$$V_{sy} = V_{ay}^{e} + \left(V_{az}^{e} \sin\gamma - r_l \frac{d\gamma_a'}{dt} \right) \frac{1}{\cos\gamma} \tag{10.35}$$

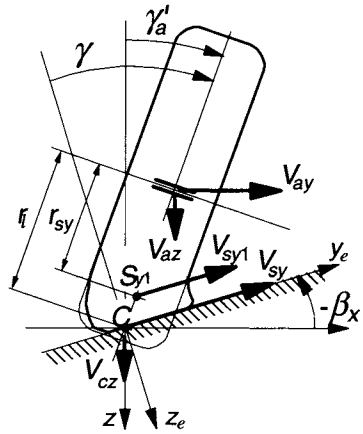

Fig. 10.31. Side slip velocity components at road and wheel camber.

$$V_{sy1} = V_{ay}^{e} - \left\{ r_{sy} \frac{\mathrm{d}\gamma_a'}{\mathrm{d}t} + (r_l - r_{sy}) \frac{\mathrm{d}\beta_x}{\mathrm{d}t} \right\} \cos\gamma \tag{10.36}$$

where $V_{ay,z}^{e}$ represents the axle velocity components parallel to the current effective road system of axes (x_e, y_e, z_e).

In Fig.10.32 example results are presented of experimental and model

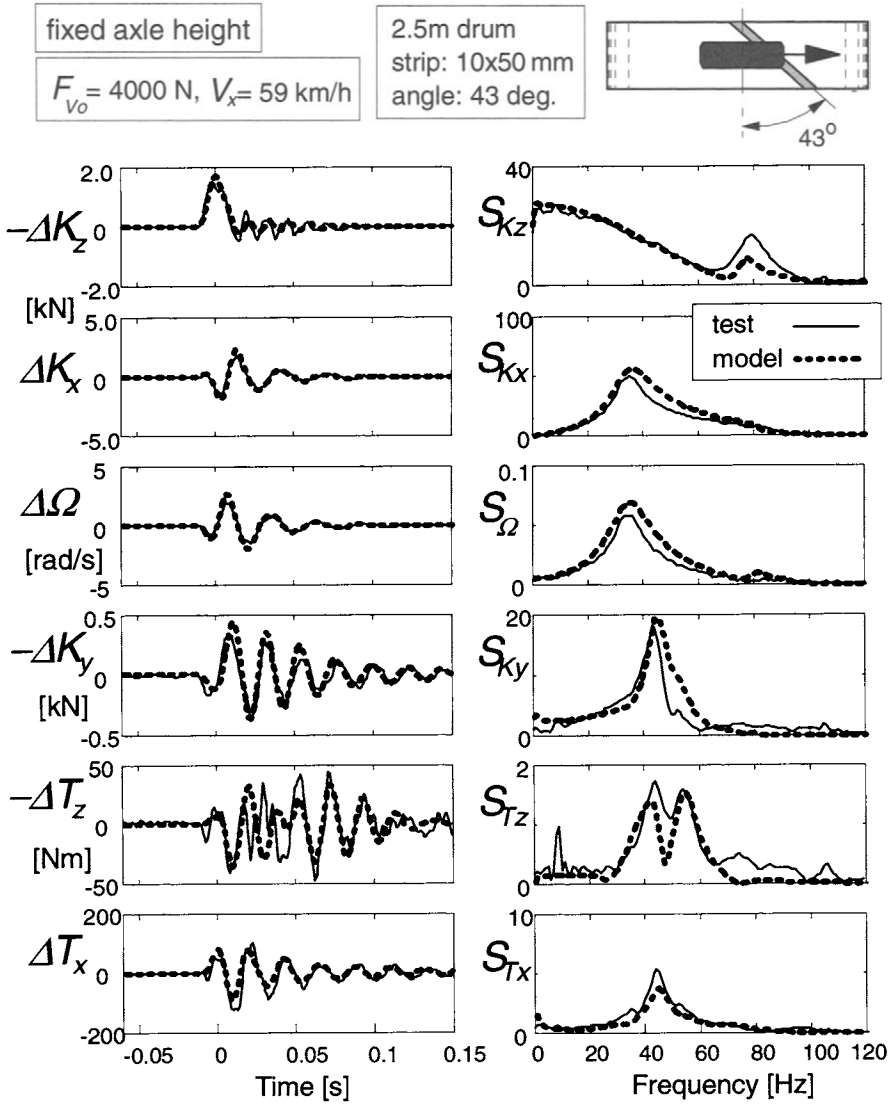

Fig. 10.32. Running over an oblique cleat (10x50mm strip) mounted on the drum surface at an angle of 43 degrees, at constant axle height. Measured and computed variations of wheel spindle forces K and moments T and wheel angular speed Ω versus time and as power spectral densities S.

simulation results of the tyre moving at constant axle height at a speed of 59 km/h over an oblique strip (height 10 mm, width 50 mm) mounted at an angle of 43 degrees with respect to the drum axis (wheel slip angle and wheel camber angle remain zero). The variations of the wheel spindle forces $K_{x,y,z}$ and moments $T_{x,z}$ and the wheel angular velocity Ω are presented as functions of time and as power spectral densities versus frequency. Note: the output forces and moments $K_{x,y,z}$ and $T_{x,z}$ are the same as the quantities $K_{a\xi,\eta,\zeta}$ and $T_{a\xi,\zeta}$ expressed by the equations (9.195-9.200), also cf. Fig.9.25. Again, it is seen that a reasonable or good correspondence can be achieved. The various tyre-wheel resonance frequencies can be observed to show up: vertical mode at 78Hz (K_z), rotational mode at 35Hz (K_x and Ω), camber mode at 46Hz (K_y, T_z and T_x) and yaw mode at 54Hz (T_z).

10.2. Three Advanced Dynamic Tyre Models: *SWIFT, FTire, RMOD-K*

Three relatively recent and advanced dynamic tyre models have been discussed at a CCG Seminar held at the Technical University in Vienna, September 2004. These commercially available models are: *FTire*, *RMOD-K* and *SWIFT*. The present section gives a comparative outline of these models. For further study we may refer to the original seminar material, cf. CCG (2004). The text below is largely reproduced from Chapter 2 of the state-of-the-art paper by Lugner, Pacejka and Plöchl (2005).

Outline of the Three Dynamic Models

The three models manifest different ways of approach, different levels of complexity and as a result differences in computational effort. Agreement with experimental data may be significantly different depending on the type of application. The three models all aim at similar motion input ranges and types of application. These include: steady-state (combined) slip, transients and higher frequency responses, covering at least the rigid body modes of vibration of the tyre belt. The models are designed to roll over three-dimensional road unevennesses, typically exhibiting the enveloping properties of the tyre. In addition, the models can cover situations where the forward speed vanishes, its sign may reverse and parking manoeuvres may follow. Moreover, the models can handle moving road surfaces.

The program packages offer simplified and/or more refined versions that may

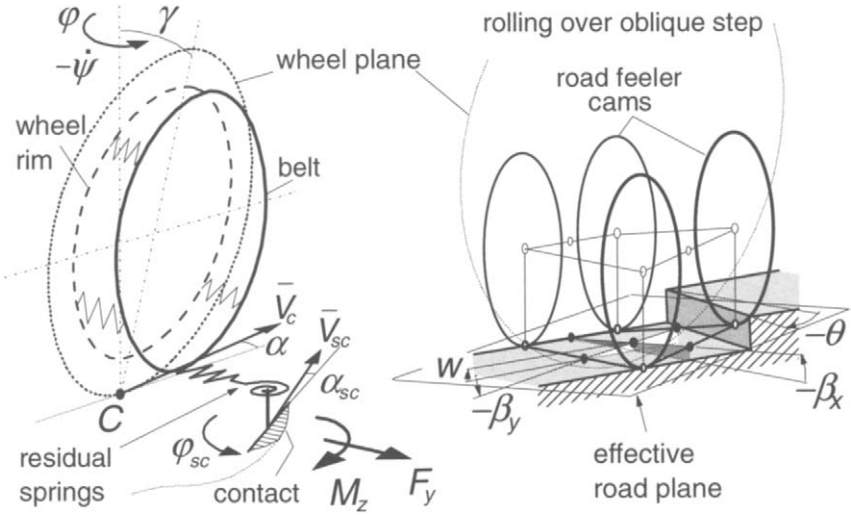

Fig. 10.33. General configuration of the *SWIFT* model featuring rigid belt ring, residual stiffnesses, contact patch slip model and double-track tandem-cam road feeler with resulting effective road inputs.

be chosen depending on less or more demanding types of application. Of course, considerable differences in required CPU time are involved.

SWIFT (or in the context of *Delft-Tyre*: *MF-Swift*) is a model of relative simplicity in representing the actual physical structure of the tyre. However, the model relies heavily on experimental evidence concerning the tyre-road slip properties, thereby enabling the generation of slip characteristics of unmatched accuracy (*Magic Formula*). The belt is represented by a rigid ring with residual springs that connect the ring with the contact patch, cf. Fig.10.33. This simplification limits the model bandwidth to ca. 80Hz. Contact dynamic behaviour is represented by an approximate description of the exact frequency response characteristics of the non-linear brush model. The wavelength of horizontal tyre motions is limited to not less than ca. 10cm. Rolling over road unevennesses is accomplished through the introduction of the so-called effective road plane that is defined by the vertical positions of a 2-d tandem or 3-d multiple set of oval cams that move over the actual, possibly sharp edged road surface. Scaling factors can be used to handle changes that may occur in e.g. frictional and service conditions. Besides the common over the road full-scale tyre slip measurements, some special tests and straightforward rolling experiments, notably over (oblique) cleats, to determine parameters pertaining to dynamic rolling behaviour are required. Approximate estimation of a part of the parameters is a possible popular alternative. The much simpler but faster *Magic Formula* quasi-steady-state or transient tyre model, *MF-Tyre*, is limited

to ca. 10Hz, relatively large motion wavelengths and smooth road surfaces. At steady-state, *SWIFT* becomes identical to this simpler version. Easy switching from the simplest to the most complex dynamic 3-d versions is possible. Parameterisation and visualisation is made simple through the use of *MF-Tool*. More information on *MF-Swift* can be found in the preceeding sections of the present chapter and through *Delft-Tyre*.

The model *FTire*, cf. Gipser et al. (1997) and Gipser (1999), features a flexible belt provided with a large number of friction elements (on tread blocks). The flexible belt is modelled by 80 to 200 segments each possessing five degrees of freedom, including twist and bending (about circumferential axis). They are connected mutually and with respect to the wheel rim by non-linear spring-damper elements, cf. Fig.10.34. To each of the segments 1000 to 10000 friction elements are attached through 5 to 50 tread blocks. Through these elements normal and frictional forces are generated. Friction functions are used that make distinction between stitching and sliding friction. The tread blocks may represent

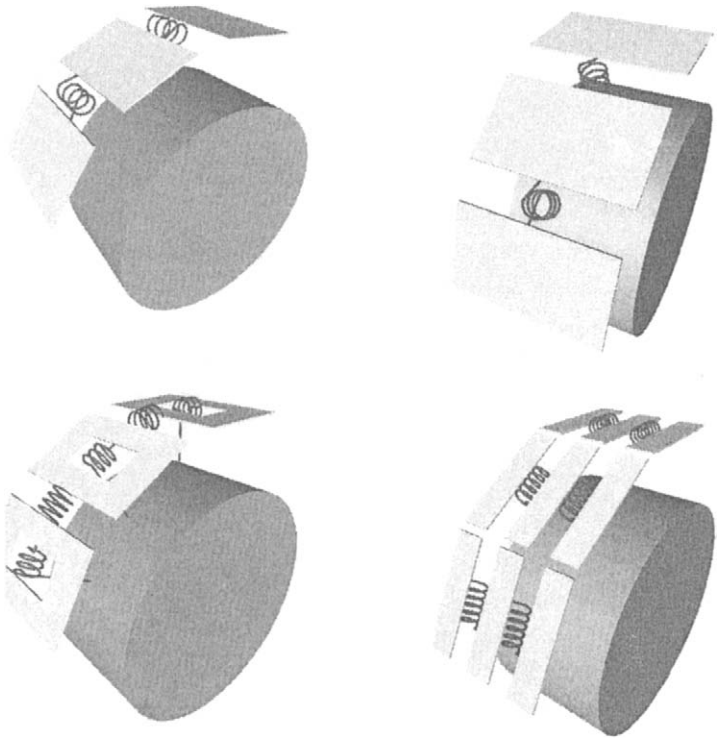

Fig. 10.34. *FTire* flexible belt representation by a number of segments elastically attached to each other and to the wheel rim. Segments are provided with tread blocks.

(simple) tread pattern designs. A thermal model can give rise to changes in temperature of structure and contact surface, thereby varying friction and inflation pressure and thus stiffness properties. In addition, the model features a tread wear model based on the concept of friction power. The contact patch contour and pressure distribution follow from the model's flexible properties. The model can roll over arbitrary uneven, possibly sharp edged, road surfaces. The band width of the model is limited to ca. 150Hz (up to first-order bending modes). Horizontal motion wavelengths to not smaller than 5 to 15cm. Special measurements are required to assess geometry, inertia and stiffness/damping, friction and material properties. Parameterisation may be conducted with the aid of (oblique) cleat tests or through estimation schemes or by calculations with *FETire*, a finite element detailed tyre model. A much simpler, rigid belt, model is available for much faster computations but limited to 100Hz and relatively smooth surfaces with wavelengths larger than twice the contact patch length. Data compatibility and interface enables easy switching between models. A handling and fitting tool is available.

The model *RMOD-K*, cf. Oertel (1997) and Oertel and Fandre (1999), gives a detailed finite element description of the actual tyre structure, Fig.10.35. It features a flexible belt that is connected to the rim with a simplified, preprocessed, sidewall model with pressurised air. The belt is modelled by one or more layers that interact with each other. Road contact is realised through an additional sensor layer. In sensor points the normal and frictional forces are calculated. The contact area, with possible gaps, and pressure distribution result from the rolling and compressed model calculations. The complexity of the

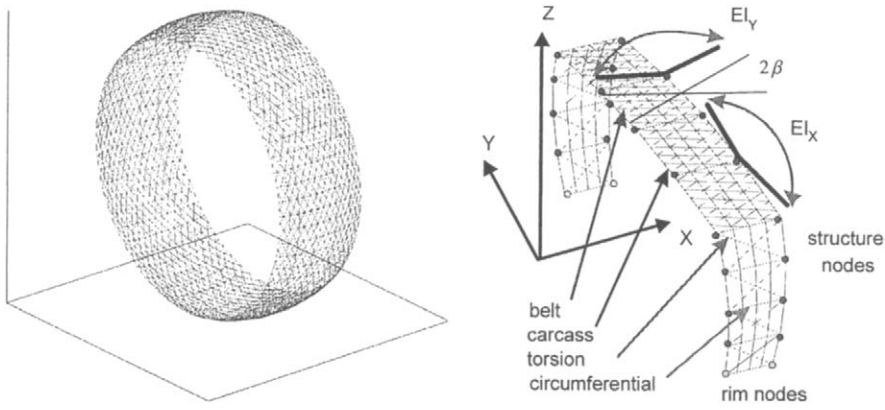

Fig. 10.35. *RMOD-K* finite element structure representation. Belt mesh and complete cross section element.

model may be reduced depending on the type of application: from fully FEM to hybrid and discretised structure representations. Three-dimensional uneven road surfaces can be dealt with very well with this sophisticated model. The computational effort, however, remains relatively high. Friction functions are included that allow the generation of both adhesion and sliding areas with friction levels that depend on temperature (WLF transformation) and contact pressure. A very much simpler model is available that is based on a rigid belt representation and a separate model for the calculation of the footprint dimensions and the pressure distribution. Contact dynamics is analytically treated in the areas of adhesion. Applications are limited to smooth roads and ca. 100Hz. Also for these models handling and fitting aids are available.

Remarks

Obviously, the complex physically based models are better suited to examine the effects of the change of a physical parameter such as material stiffness and cross section contour. The more empirically oriented models are better equipped to investigate the effect of changing performance parameters such as cornering and vertical stiffnesses without affecting remaining properties.